

Non-locality of the Turbulent Electromotive Force

Abhijit B. Bendre,^{1,2*} Kandaswamy Subramanian,^{2†}

¹*École polytechnique fédérale de Lausanne - EPFL, Switzerland*

²*IUCAA, Post Bag 4, Ganeshkhind, Pune 411007, India*

2 August 2021

ABSTRACT

The generation of large-scale magnetic fields ($\overline{\mathbf{B}}$) in astrophysical systems is driven by the mean turbulent electromotive force ($\overline{\mathcal{E}}$), the cross correlation between local fluctuations of velocity and magnetic fields. This can depend non-locally on $\overline{\mathbf{B}}$ through a convolution kernel K_{ij} . In a new approach to find K_{ij} , we directly fit the time series data of $\overline{\mathcal{E}}$ versus $\overline{\mathbf{B}}$ from a galactic dynamo simulation using singular value decomposition. We calculate the usual turbulent transport coefficients as moments of K_{ij} , show the importance of including non-locality over eddy length scales to fully capture their amplitudes and that higher order corrections to the standard transport coefficients are small in the present case.

Key words: Magnetohydrodynamics (MHD) – ISM: magnetic fields – Galaxies: magnetic fields – dynamo – methods: numerical

1 INTRODUCTION

A persistent theme applicable in many physical contexts is the influence of small-scale, or unresolved physics, on larger scales (Krause & Rädler 1980; Bhat et al. 2016; Meneveau & Katz 2000; Gotoh & Yeung 2012; Aiyer et al. 2017; Baumann et al. 2012). This is also of crucial importance for understanding the origin of large-scale magnetic fields in stars and galaxies, ordered on scales larger than the turbulent motions. They are thought to be maintained by a mean field turbulent dynamo, through the combined action of helical turbulence and differential rotation. Their evolution is described by mean-field electrodynamics (Rädler 1969; Moffatt 1978; Krause & Rädler 1980; Shukurov & Subramanian 2021; Brandenburg & Subramanian 2005), where the velocity field \mathbf{U} and magnetic field \mathbf{B} are decomposed as the sums of their mean or large-scale (with over-line) and fluctuating or small-scale parts, $\mathbf{U} = \overline{\mathbf{U}} + \mathbf{u}$ and $\mathbf{B} = \overline{\mathbf{B}} + \mathbf{b}$. The mean (or average) is often defined over a suitable domain such that the Reynolds' averaging rules are satisfied. The evolution of $\overline{\mathbf{B}}$ is then determined by the averaged induction equation,

$$\frac{\partial \overline{\mathbf{B}}}{\partial t} = \nabla \times (\overline{\mathbf{U}} \times \overline{\mathbf{B}} + \overline{\mathcal{E}} - \eta_m \nabla \times \overline{\mathbf{B}}), \quad (1)$$

where η_m is the microscopic diffusivity. Crucially, the generation of the large-scale or mean magnetic field (and its turbulent transport) is driven by a new contribution in Eq. (1), the mean turbulent electromotive force (EMF), $\overline{\mathcal{E}} = \overline{\mathbf{u} \times \mathbf{b}}$, which depends on the cross-correlation between the turbulent velocity and magnetic fields. The determination of $\overline{\mathcal{E}}$ in terms of the mean fields themselves, either analytically using closure theory (Krause & Rädler 1980; Pouquet et al. 1976; Dittrich et al. 1984; Shukurov & Subramanian 2021; Blackman & Field 2002;

Rädler et al. 2003; Brandenburg & Subramanian 2005) or in simulations (Brandenburg & Sokoloff 2002; Schrunner et al. 2005; Simard et al. 2016; Tobias & Cattaneo 2013; Brandenburg 2018), is the key to understand mean-field dynamos.

2 TURBULENT TRANSPORT COEFFICIENTS FROM $\overline{\mathcal{E}}$

A widely used local representation of the turbulent EMF, assumes that $\overline{\mathcal{E}}$ can be expanded in terms of the mean magnetic field and its derivative. In the current work, we use a planar, xy average, to define mean fields, and then the turbulent EMF can be written as

$$\overline{\mathcal{E}}_i(z, t) = \alpha_{ij} \overline{B}_j - \eta_{ij} (\nabla \times \overline{\mathbf{B}})_j, \quad (2)$$

with the indices i and j representing either x or y components, and the mean field having only a z dependence. Here, α_{ij} and η_{ij} are turbulent transport tensors. When Lorentz forces are small and in the isotropic limit, these tensors are diagonal; $\alpha_{ij} = \alpha_0 \delta_{ij}$, $\eta_{ij} = \eta_t \delta_{ij}$; then α_0 or the α -effect is proportional to the helicity of the turbulence and the turbulent diffusivity η_t is proportional to its energy. Although, a number of different approaches have been used to estimate these coefficients even outside the isotropic limit, a majority assume this locality of the EMF. However, such an approximation is only valid when there is sufficient scale separation between the large-scale field and the turbulent velocity and ignores higher order derivatives of \overline{B}_i .

More generally $\overline{\mathcal{E}}$ can be expressed in the form of a convolution with the mean field itself (eg. Rädler 1969; Brandenburg & Subramanian 2005; Rädler 2014; Brandenburg 2018),

$$\overline{\mathcal{E}}_i(z, t) = \int_{-\infty}^{\infty} K_{ij}(z, \zeta, t) \overline{B}_j(z - \zeta, t) d\zeta. \quad (3)$$

This representation allows for the contribution of the mean magnetic field to the turbulent EMF in a non-local manner. For simplicity,

* E-mail: abhijit.bendre@epfl.ch

† E-mail: kandu@iucaa.in

we assume in this work that the time dependence is still local¹. Note that the convolution kernel K_{ij} depends both on z and a neighbourhood variable ζ separately, allowing for the inhomogeneity of magnetohydrodynamic turbulence in the general case. We will also see below that K_{ij} falls off sufficiently rapidly with ζ that the limits of integration is effectively $\pm l/2$, where l is order of the outer scale of turbulence. The more widely used local formulation, given by Eq. (2), can be recovered by Taylor expanding $\bar{\mathbf{B}}_j$ in Eq. (3) about z in powers of ζ and retaining the leading two terms. This allows the dynamo coefficients α_{ij} and η_{ij} to be expressed in terms of the zeroth and first moments of K_{ij} as

$$\begin{aligned} \begin{bmatrix} \alpha_{xx} & \alpha_{xy} \\ \alpha_{yx} & \alpha_{yy} \end{bmatrix} &= \int_{-l/2}^{+l/2} \begin{bmatrix} K_{xx} & K_{xy} \\ K_{yx} & K_{yy} \end{bmatrix} d\zeta \\ \begin{bmatrix} \eta_{xx} & \eta_{xy} \\ \eta_{yx} & \eta_{yy} \end{bmatrix} &= \int_{-l/2}^{+l/2} \begin{bmatrix} -K_{xy} & K_{xx} \\ -K_{yx} & K_{yy} \end{bmatrix} \zeta d\zeta. \end{aligned} \quad (4)$$

Similarly, the subsequent higher order moments of the kernel multiply higher derivatives of $\bar{\mathbf{B}}$. The leading higher order corrections to α_{ij} which we denote by α_{ij}^h and η_{ij} which we denote by η_{ij}^h are,

$$\begin{aligned} \begin{bmatrix} \alpha_{xx}^h & \alpha_{xy}^h \\ \alpha_{yx}^h & \alpha_{yy}^h \end{bmatrix} &= \int_{-l/2}^{+l/2} \begin{bmatrix} K_{xx} & K_{xy} \\ K_{yx} & K_{yy} \end{bmatrix} \zeta^2 d\zeta \\ \begin{bmatrix} \eta_{xx}^h & \eta_{xy}^h \\ \eta_{yx}^h & \eta_{yy}^h \end{bmatrix} &= \int_{-l/2}^{+l/2} \begin{bmatrix} -K_{xy} & K_{xx} \\ -K_{yx} & K_{yy} \end{bmatrix} \zeta^3 d\zeta. \end{aligned} \quad (5)$$

These multiply respectively the second and third derivatives of $\bar{\mathbf{B}}_j$ in the Taylor expansion of Eq. (3). Our aim here is to compute K_{ij} from the data of direct numerical simulations (DNS), examine the extent of its spatial non-locality and also derive in a novel manner, the dynamo coefficients as the moments of these components. For this we use a galactic dynamo simulation, (performed using the NIRVANA MHD code Ziegler (2008)), where supernovae (SN) introduced at randomly chosen points in the simulation box drive a multi-phase turbulent flow in the medium.

3 DESCRIPTION OF THE DIRECT SIMULATIONS

The details of the galactic dynamo simulations have been described in Bendre et al. (2015); Bendre (2016); Bendre et al. (2020); here we only summarize some features. Specifically, to have a reasonable comparison with the current determination of transport coefficients we use a run Q which has been analysed previously for this purpose using different methods, the test-field (TF) method² (Bendre et al. 2015), a local linear regression method and a local version of the singular value decomposition (SVD) method (Bendre et al. 2020). The DNS model we use is a local Cartesian shearing box of ISM (with $L_x = L_y = 0.8$ kpc, and -2.12 kpc to $+2.12$ kpc in the z direction), split in $96 \times 96 \times 512$ grids with a resolution of ~ 8.3 pc. Shearing periodic boundary conditions are used in the radial (x) direction to incorporate the differential rotation. While the flat rotation curve is simulated by letting angular velocity scale as $\Omega \propto 1/R$ with the radius, with a value of $\Omega_0 = 100$ km s⁻¹ kpc⁻¹ at the centre of the domain. In z direction outflow conditions are used to let the gas

¹ See Hubbard & Brandenburg (2009); Rheinhardt & Brandenburg (2012a) where time non-locality is explored using the test-field method

² For an extensive discussion of the TF method and its applications in several contexts see Schrunner et al. (2005, 2007); Brandenburg (2005); Sur et al. (2008); Gressel et al. (2008); Käpylä et al. (2009); Bendre et al. (2015); Gressel & Pessah (2015); Warnecke et al. (2018).

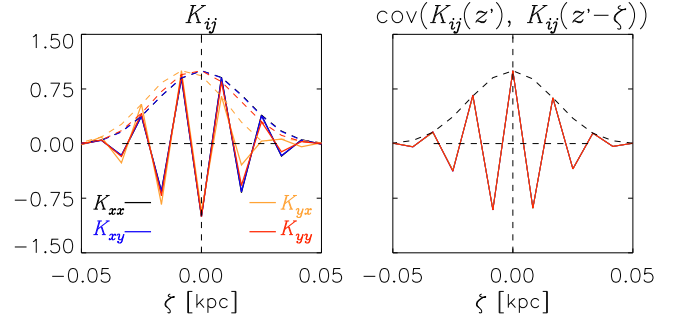


Figure 1. The left panel shows the normalized values of the convolution kernel K_{ij} (solid lines) and its absolute value (dashed lines) at a representative $z' = 500$ pc. The right panel shows the normalized covariance of K_{xx} (solid line) and its absolute value (dashed line) between the point $\zeta = 0$ (also at $z' = 500$ pc) and that at a neighbouring ζ .

escape, while preventing its inflow. SN explosions are simulated as expulsions of thermal energy at randomly chosen locations in the box at a rate of ~ 7.5 kpc⁻² Myr⁻¹. Furthermore the distribution of SN explosion locations is also scaled with the vertical profile of mass density. As an initial condition we use a vertically stratified density profile, such that the system is in a hydrostatic equilibrium, with a balance between gravitational and pressure gradient forces. This leads to a scale height of ~ 300 pc for the density (and a midplane value of 10^{-24} g cm⁻³). Additionally, a piece-wise power law is also used to describe the temperature dependent radiative cooling. This, along with SN explosions, leads the plasma splitting into multiple thermal phases within a few Myr, which roughly captures the ISM morphology.

The initial magnetic field is of a strength of about 10^{-9} G (about 3-4 orders of magnitude smaller than the equipartition strength), Both the total and mean magnetic field amplify exponentially with an e-folding time of ~ 200 Myr. The mean magnetic field goes through a several reversals and parity changes until finally reaching to a large scale mode vertically symmetric about the mid plane. Within about a Gyr they reach μ G strengths, in equipartition with the turbulent kinetic energy density. Subsequently the magnetic energy continues to grow at about 5 times smaller growth rate. The time evolution of magnetic energy density and $\bar{\mathbf{B}}(z, t)$ are shown respectively in Fig. 9 and Fig. 10 of Bendre et al. (2020).

4 DETERMINING THE NON-LOCAL KERNEL

To determine the components K_{ij} using the SVD method we proceed as follows. We first extract the time series of $\bar{\mathbf{B}}_j(z, t)$ and $\bar{\mathbf{E}}_j(z, t) = \overline{(\mathbf{u} \times \mathbf{b})}_j$ at each z and ranging from approximately 0 to 900 Myr in time, corresponding to the kinematic phase of the dynamo (comprising of 800 points in total). We then express Eq. (3) at any particular $z = z'$ in the form of a discrete sum,

$$\bar{\mathbf{E}}_i(z', t) = \sum_{n=-m}^m K_{ij}(z', \zeta_n, t) \bar{\mathbf{B}}_j(z' - \zeta_n, t) \epsilon \quad (6)$$

where $\zeta_n = n\epsilon$ denotes the location of mesh points in the local neighbourhood of and including z' , with the index n ranging from $-m$ to $+m$, and ϵ the size of the simulation mesh. The value of m fixes the width of the local neighbourhood and it is expected that the coefficients K_{ij} would vanish for a large enough m , such that $m\epsilon$ is larger than the eddy length scales. We have explored values of $m \leq 6$

equivalent of a local neighbourhood of about -50 to 50 pc. This turns out to be sufficient as discussed below and seen from Fig. 1.

For $m = 6$, Eq. (6) then represents a system of 2 equations in 26 unknowns (6 points on either sides of each $z = z'$) which we solve by using a time series analysis. We assume that the coefficients K_{ij} do not vary in time during the initial kinematic phase of the dynamo, when Lorentz forces are negligible which is justifiable as discussed in our previous analysis (Bendre et al. 2020). This allows us to express Eq. (6) at each $z = z'$ and times $(t_1, t_2 \dots t_N)$ as an over-determined system of linear equations between \mathcal{E} and \mathbf{B} . To solve this system for K_{ij} using SVD, we first write Eq. (6) in a matrix form, $\mathbf{y}_i = \mathbf{A} \cdot \mathbf{x}_i + \hat{\mathbf{n}}_i$ (i is either x or y), where the matrix $\hat{\mathbf{n}}_i$ represents an additive noise in the determination of the vector \mathbf{y}_i . Here

$$\mathbf{y}_i^\top = \left[\bar{\mathcal{E}}_i(z', t_1) \quad \bar{\mathcal{E}}_i(z', t_2) \quad \dots \quad \bar{\mathcal{E}}_i(z', t_N) \right]$$

$$\mathbf{A}^\top = \begin{bmatrix} \bar{B}_x(z' - 6\epsilon, t_1) & \bar{B}_x(z' - 6\epsilon, t_2) & \dots & \bar{B}_x(z' - 6\epsilon, t_N) \\ \vdots & \vdots & & \vdots \\ \bar{B}_x(z' + 6\epsilon, t_1) & \bar{B}_x(z' + 6\epsilon, t_2) & \dots & \bar{B}_x(z' + 6\epsilon, t_N) \\ \bar{B}_y(z' - 6\epsilon, t_1) & \bar{B}_y(z' - 6\epsilon, t_2) & \dots & \bar{B}_y(z' - 6\epsilon, t_N) \\ \vdots & \vdots & & \vdots \\ \bar{B}_y(z' + 6\epsilon, t_1) & \bar{B}_y(z' + 6\epsilon, t_2) & \dots & \bar{B}_y(z' + 6\epsilon, t_N) \end{bmatrix}$$

$$\mathbf{x}_i = \begin{bmatrix} K_{ix}(z', +6\epsilon) \\ \vdots \\ K_{ix}(z', -6\epsilon) \\ K_{iy}(z', +6\epsilon) \\ \vdots \\ K_{iy}(z', -6\epsilon) \end{bmatrix}$$

and $N = 800$ is the length of the time series. Furthermore, $\bar{\mathbf{B}}$ at the m points outside the top and bottom of the boundaries is set to zero; however, adopting reflecting boundaries at the top and bottom, has negligible effect on the final results.

We find the least square solution to the matrix relation $\mathbf{y}_i = \mathbf{A} \cdot \mathbf{x}_i + \hat{\mathbf{n}}_i$ by pseudo-inverting the design matrix \mathbf{A} using the SVD algorithm. Specifically the matrix \mathbf{A} is represented as a singular value decomposition $\mathbf{A} = \mathbf{U} \mathbf{w}^{-1} \mathbf{V}^\top$, where \mathbf{U} and \mathbf{V} are orthonormal matrices of dimension $(N \times 26)$, and (26×26) while \mathbf{w} is a 26×26 diagonal matrix. The least square solution, denoted by $\hat{\mathbf{x}}_i$, is then determined simply by, $\hat{\mathbf{x}}_i = \mathbf{V} \mathbf{w} \mathbf{U}^\top \mathbf{y}_i$ (Mandel 1982; Press et al. 1992). Note that \mathcal{E} and \mathbf{B} grow exponentially as $\exp(t/200\text{Myr})$ during the kinematic stage even as K_{ij} remains constant. This growth is scaled out of \mathbf{y}_i and the columns of \mathbf{A} before implementing the SVD algorithm to find $\hat{\mathbf{x}}_i$, as in our earlier work (Bendre et al. 2020).

The SVD analysis also gives the full covariance matrix between the l^{th} and m^{th} element of $\hat{\mathbf{x}}_i$,

$$\text{Cov}([\hat{\mathbf{x}}_i]_l, [\hat{\mathbf{x}}_i]_m) = \sum_{j=0}^{25} \frac{\mathcal{V}_{lj} \mathcal{V}_{mj}}{\mathbf{w}_{jj}^2} \sigma_i^2. \quad (7)$$

Here σ_i is the 1σ variance associated the vector \mathbf{y}_i ,

$$\sigma_i^2 = \frac{1}{N} (\mathbf{y}_i - \mathbf{A} \hat{\mathbf{x}}_i)^\top (\mathbf{y}_i - \mathbf{A} \hat{\mathbf{x}}_i). \quad (8)$$

The diagonal ($l = m$) elements in Eq. (7) give the variance in the l^{th} element in the vector of $\hat{\mathbf{x}}_i$ and so determines the 1σ errors in each component of the kernel K_{ij} . However, to determine the errors in the various moments of the kernel (Eq. (4)), the fact that components K_{ij} are correlated within the ζ neighbourhood also needs to be accounted for. Consider any of the turbulent transport

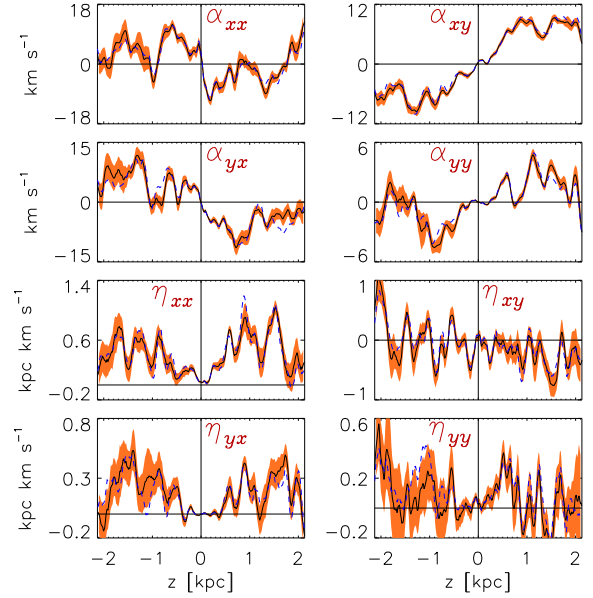


Figure 2. Blue dashed lines show the vertical profiles of the zeroth and first moments of the kernel K_{ij} calculated non-locally using Eq. (4) with the SVD method. We have adopted $m = 6$, equivalent to the local neighbourhood of size ± 50 pc. Shown in black solid lines are the same profiles but calculated using nine different sections of time series S_1 to S_9 . Orange shaded regions indicate the 1σ errors for these nine realizations.

coefficients, say Z , which is written as the sum $Z = \sum_{m=-6}^6 z_m$. Then the variance $\text{Var}(Z) = \sum_m \sum_n \text{Cov}(z_n, z_m)$ and the 1σ error in Z can be calculated as $\sqrt{\text{Var}(Z)}$.

In the left panel of Fig. 1 we show the normalized coefficients of the recovered convolution kernel K_{ij} (solid lines) and their absolute values (dashed lines), as functions of ζ at a representative $z' = 500$ pc. We see that all coefficients drop to negligible values within $\zeta = \pm 50$ pc, which is also their approximate half widths. This scale is in fact of order of the correlation scale of interstellar medium turbulence in the simulations of Bendre et al. (2015); Hollins et al. (2017). The right hand panel shows the normalised covariance (solid line) and its absolute value (dashed line) for K_{xx} , between its value at $\zeta = 0$ (also at $z' = 500$ pc) and that at an arbitrary neighbourhood point ζ . Again, we see that these profiles too vanish smoothly at the boundaries of the chosen local neighbourhood. As the coefficients $K_{ij}(z', \zeta)$ are correlated within the local neighbourhood, and determined only in the least-square sense, their amplitude at a particular ζ has correlated errors. However, the extent of non-locality of $\bar{\mathcal{E}}$, is well constrained by the width of the dashed profiles in the left hand panel of Fig. 1.

5 TURBULENT TRANSPORT COEFFICIENTS

Once the kernel components $K_{ij}(z, \zeta)$ are determined, the transport coefficients α_{ij}, η_{ij} , are obtained by calculating the first two moments of the kernel as in Eq. (4) after converting the integrals to discrete sums over ζ_n with n ranging between $\pm m$. The vertical (z -dependent) profiles of these coefficients are shown in Fig. 2 as dashed lines. The 1σ SVD error in their determination, calculated from its variance as described above by summing over all the corresponding elements of the covariance matrix, turns out to be very small, less than 2–3% of the coefficients themselves. This is both due to cancellations when summing over the signed covariances in $\sum_m \sum_n \text{Cov}(z_n, z_m)$, and

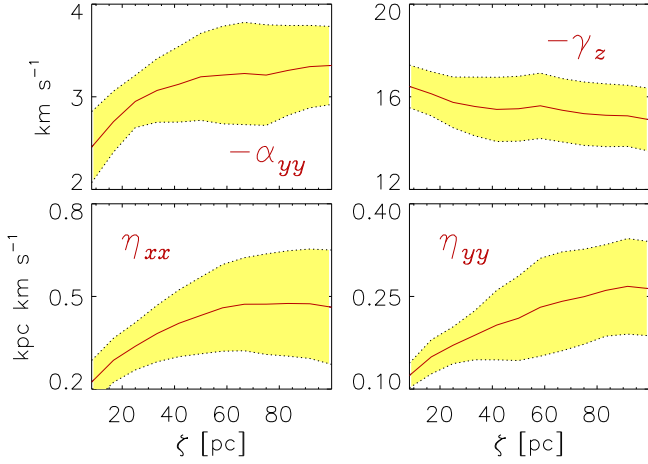


Figure 3. The solid red lines are various turbulent transport coefficients as functions of the half width of local neighbourhood (Fig. 2 corresponds to the width of 50 pc). All the coefficients are averaged at the vertical location $z = 1 \text{ kpc} \pm 100 \text{ pc}$, except for α_{yy} which is taken at $z = -1 \text{ kpc} \pm 100 \text{ pc}$, since its vertical profile has a fluctuation at around $\sim 0.8 \text{ kpc}$, (eg. Fig. 2). Shaded in yellow are the regions corresponding to width of one mean absolute deviation.

because the term σ_i^2 in Eq. (7) is small as it depends inversely on N . As an alternate measure of the error, we split the time series into nine different time series (S_1 to S_9) by extracting points that are about a correlation time apart (8 points in the time series) as in Bendre et al. (2020). We then use the SVD to determine K_{ij} for each of these time series and compute its moments to determine α_{ij} and η_{ij} . The mean of these 9 realizations is shown as solid lines in Fig. 2 and agrees well with that computed from the full series. The orange shaded regions in Fig. 2, indicate the error on the mean estimated as the variance divided by the number of realizations (see for example Press et al. (1992)). We note that widening the size of local neighbourhood amounts to the determination of more unknown K_{ij} 's in the system, which increases errors in the determination of transport coefficients. Moreover, $\bar{\mathcal{E}}_y$ and \bar{B}_x are noisier in the DNS compared to their counterparts, and therefore the coefficients α_{yx} and η_{yy} , that depend on these two, are noisier compared to the other coefficients.

The z -dependencies of turbulent coefficients in Fig. 2 are quite similar to their local determination in Bendre et al. (2020); however several of them, like η_{ij} and α_{yy} have larger amplitudes. In fact we find that the vertical profiles of the dynamo coefficients determined adopting $m = 1$ match very well with that determined from the same simulation using our previous local SVD analysis Bendre et al. (2020). To examine the importance of non-locality more carefully, we vary the size of local neighbourhood in Eq. (6), ranging from $m = 1$ to 12 (about $\pm 8 \text{ pc}$ to $\pm 100 \text{ pc}$), and determine the components of K_{ij} for each of those cases. The results are shown in Fig. 3 (as solid red lines), by averaging the coefficients at $z = 1 \text{ kpc} \pm 100 \text{ pc}$, except for α_{yy} which is averaged over $z = -1 \text{ kpc} \pm 100 \text{ pc}$. Shaded in yellow are the regions corresponding to width of one mean absolute deviation. We see that α_{yy} , crucial for the generation of \bar{B}_x from \bar{B}_y , and the turbulent diffusion coefficients η_{xx} , η_{yy} all increase with the size of neighbourhood until $m \sim 6$ (equivalent to $\sim \pm 50 \text{ pc}$), and stabilize thereafter (to the profiles shown in of Fig. 2). The turbulent diamagnetic pumping term $\gamma_z = (\alpha_{yx} - \alpha_{xy})/2$, which leads to a vertical advection of the mean field also appears to stay constant with m after initially decreasing up to $m \leq 6$. This indi-

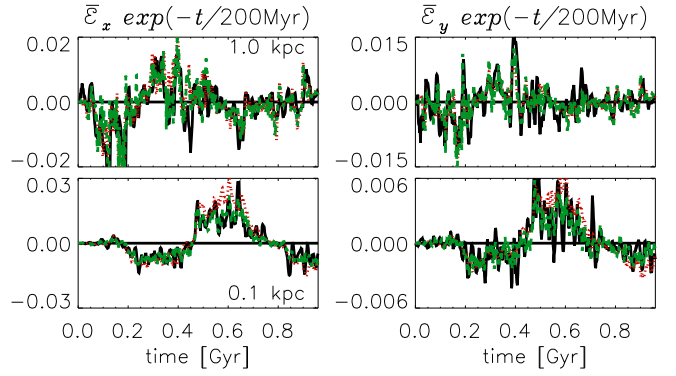


Figure 4. Shown in the left and right hand panels respectively, with black solid lines, are the time series of x and y components of EMF, as obtained from the DNS, at $z = 1 \text{ kpc}$ (top panels) and $z = 0.1 \text{ kpc}$ (bottom panels). The green dashed lines show the same EMF time series but as reconstructed using Eq. (3), while the red dotted lines show the EMF time series using only first two moments of the kernel (i.e. α_{ij} and η_{ij}). EMF components are expressed in the units of $\mu \text{ G km s}^{-1}$, and additionally we have scaled their time series with a factor $\exp(-t/200 \text{ Myr})$ to account for the exponential growth of $\bar{\mathcal{E}}_i$.

cates the importance of the non-local contributions included here, that are ignored when using Eq. (2) or too small a value of m to compute the coefficients. The asymptotic values of these transport coefficients compare favorably with theoretical expectations for the galactic interstellar medium, and can lead to the large-scale dynamo action seen in this simulation, as already discussed in Bendre et al. (2020). The trends seen in Fig. 3 are also qualitatively consistent with Brandenburg et al. (2008); Rheinhardt & Brandenburg (2012b) and specifically the work of (Gressel & Elstner 2020), where the scale-dependence of the transport coefficients was obtained by varying the wave-number of test-fields (used to measure them) from $k = 1$ (equivalent to the box size of $\sim 4 \text{ kpc}$) to $k = 32$. The present analysis, on the other hand, infers this dependence in a new direct approach by firstly using the actual mean fields instead of test fields, and also by increasing the width of the local neighbourhood, up from the grid size, to incorporate non-locality.

Finally, in Fig. 4, we compare the time series of EMF components calculated directly from the DNS (solid black line), with both the EMF reconstructed using Eq. (3) (and the recovered kernel coefficients K_{ij}) (green dashed line), and also that using Eq. (2) (red dotted line) which neglects higher order corrections to α_{ij} and η_{ij} . This is done at two representative locations. From Fig. 4, it is clear first that the non-local SVD method does indeed recover the EMF from the DNS reasonably well. Second, comparing the dashed and dotted lines in Fig. 4, we see that the inclusion of higher order terms does not significantly affect the determination of EMF, in the present galactic dynamo context. To see this explicitly, we compute α_{ij}^h , and the hyper-diffusion correction η_{ij}^h using Eq. (5) after converting it to discrete sums. In Fig. 5 we show these second and third moments of K_{ij} in the same units as α_{ij} and η_{ij} . This has been done by dividing them by L^2 , where $L = 0.2 \text{ kpc}$ is of order of the scale over which the mean magnetic field varies. It can be seen by comparing Fig. 5 with Fig. 2, that these higher order contributions are of order a few percent of α_{ij} and η_{ij} . This is a small correction in the present case; however such contributions could be important in other contexts.

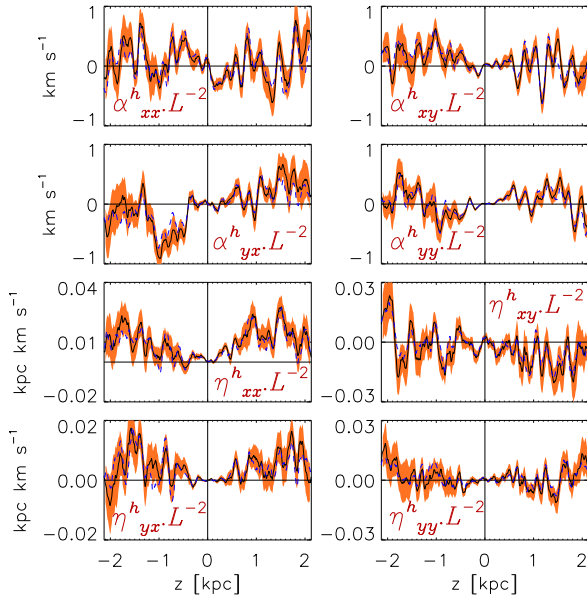


Figure 5. Shown in black solid lines are vertical profiles of α_{ij}^h and η_{ij}^h scaled with L^{-2} . These are determined by applying non-local SVD method to the time series S_1 to S_9 , same as in the Fig. 2, and averaging the outcomes. Orange regions show the errors on these means. With blue dashed lines same profiles are shown except they are calculated by taking the full time series into account.

6 CONCLUSIONS

We have shown here that the turbulent EMF depends in a non-local manner on the mean magnetic field, and determined the corresponding non-local convolution kernel $K_{ij}(z, \zeta)$ which relates the two as in Eq. (3). We do this using a new approach of least square fitting directly the time-series data of the $\bar{\mathbf{E}}$ versus $\bar{\mathbf{B}}$, from a galactic dynamo simulation, using the SVD method. We show that the non-locality extends over eddy length scales of order ± 50 pc around any fiducial location and the reconstructed $\bar{\mathbf{E}}$ using Eq. (3) matches well with that obtained directly from the simulation. The lowest order moments of K_{ij} over ζ give the standard local turbulent transport coefficients α_{ij} and η_{ij} , which however only converge when one accounts for the full extent of non-locality of K_{ij} . Higher order corrections to the standard transport coefficients are small in the present galactic dynamo simulation, but importantly, our method allows us to explicitly compute them. A caveat of the linear least-square fitting method using the SVD is that it requires \mathbf{y}_i and \mathbf{x}_i to vary over sufficiently large range (as in the present case). However, their advantages are many; of being able to use directly the simulation data without having to solve a set of auxiliary equations as in the test-field method, to handle additive noise $\hat{\mathbf{n}}$, and to determine the full covariance matrix of the of the fitted parameters. As we have shown here the method can also be generalized to determine the non-locality of transport coefficients. It would be of interest to test this method on other physical systems, not only in MHD and fluid turbulence but also in the context of any effective field theory, where subgrid physics affects larger scales.

DATA AVAILABILITY

The data underlying this article will be shared on reasonable request to the corresponding author.

ACKNOWLEDGEMENTS

We thank Axel Brandenburg, Detlef Elstner, Oliver Gressel, Aseem Paranjape, Anvar Shukurov and particularly Jennifer Schober for very useful discussions and suggestions on the paper. Abhijit B. Bendre also thanks Jennifer Schober for hosting him throughout the project at EPFL.

REFERENCES

- Aiyer A. K., Subramanian K., Bhat P., 2017, *J. Fluid Mech.*, **824**, 785
 Baumann D., Nicolis A., Senatore L., Zaldarriaga M., 2012, *Journal of Cosmology and Astroparticle Physics*, 2012, 051
 Bendre A. B., 2016, doctoralthesis, Universität Potsdam
 Bendre A., Gressel O., Elstner D., 2015, *Astronomische Nachrichten*, **336**, 991
 Bendre A. B., Subramanian K., Elstner D., Gressel O., 2020, *MNRAS*, **491**, 3870
 Bhat P., Subramanian K., Brandenburg A., 2016, *MNRAS*, **461**, 240
 Blackman E. G., Field G. B., 2002, *Phys. Rev. Lett.*, **89**, 265007
 Brandenburg A., 2005, *Astronomische Nachrichten*, **326**, 787
 Brandenburg A., 2018, *Journal of Plasma Physics*, **84**, 735840404
 Brandenburg A., Sokoloff D., 2002, *Geophys. Astrophys. Fluid Dyn.*, **96**, 319
 Brandenburg A., Subramanian K., 2005, *Physics Reports*, **417**, 1
 Brandenburg A., Rädler K. H., Schinner M., 2008, *A&A*, **482**, 739
 Dittrich P., Molchanov S. A., Sokoloff D. D., Ruzmaikin A. A., 1984, *AN*, **305**, 119
 Gotoh T., Yeung P., 2012, *Passive Scalar Transport in Turbulence: A Computational Perspective*. Cambridge University Press, p. 87–131
 Gressel O., Elstner D., 2020, *MNRAS*, **494**, 1180
 Gressel O., Pessah M. E., 2015, *ApJ*, **810**, 59
 Gressel O., Elstner D., Ziegler U., Rüdiger G., 2008, *Astronomy and Astrophysics*, **486**, L35
 Hollins J. F., Sarson G. R., Shukurov A., Fletcher A., Gent F. A., 2017, *ApJ*, **850**, 4
 Hubbard A., Brandenburg A., 2009, *ApJ*, **706**, 712
 Käpylä P. J., Korpi M. J., Brandenburg A., 2009, *Astronomy and Astrophysics*, **500**, 633
 Krause F., Rädler K.-H., 1980, *Mean-Field Magnetohydrodynamics and Dynamo Theory*. Pergamon Press (also Akademie-Verlag: Berlin), Oxford
 Mandel J., 1982, *The American Statistician*, **36**, 15
 Meneveau C., Katz J., 2000, *Annual Review of Fluid Mechanics*, **32**, 1
 Moffatt H. K., 1978, *Magnetic Field Generation in Electrically Conducting Fluids*. Cambridge Univ. Press, Cambridge
 Pouquet A., Frisch U., Leorat J., 1976, *J. Fluid Mech.*, **77**, 321
 Press W. H., Teukolsky S. A., Vetterling W. T., Flannery B. P., 1992, *Numerical Recipes in C (2Nd Ed.)*: The Art of Scientific Computing. Cambridge University Press, New York, NY, USA
 Rädler K.-H., 1969, *Veroeffentlichungen der Geod. Geophys.*, **13**, 131
 Rädler K. H., 2014, arXiv e-prints, p. arXiv:1402.6557
 Rädler K.-H., Kleorin N., Rogachevskii I., 2003, *Geophys. Astrophys. Fluid Dyn.*, **97**, 249
 Rheinhardt M., Brandenburg A., 2012a, *Astronomische Nachrichten*, **333**, 71
 Rheinhardt M., Brandenburg A., 2012b, *Astronomische Nachrichten*, **333**, 71
 Schinner M., Rädler K.-H., Schmitt D., Rheinhardt M., Christensen U., 2005, *Astronomische Nachrichten*, **326**, 245
 Schinner M., Rädler K.-H., Schmitt D., Rheinhardt M., Christensen U. R., 2007, *Geophysical and Astrophysical Fluid Dynamics*, **101**, 81
 Shukurov A., Subramanian K., 2021, *Astrophysical Magnetic Fields: From Galaxies to the Early Universe*. Cambridge Univ. Press, Cambridge
 Simard C., Charbonneau P., Dubé C., 2016, *Advances in Space Research*, **58**, 1522
 Sur S., Brandenburg A., Subramanian K., 2008, *MNRAS*, **385**, L15
 Tobias S. M., Cattaneo F., 2013, *J. Fluid Mech.*, **717**, 347
 Warnecke J., Rheinhardt M., Tuomisto S., Käpylä P. J., Käpylä M. J., Brandenburg A., 2018, *A&A*, **609**, A51
 Ziegler U., 2008, *Computer Physics Communications*, **179**, 227

This paper has been typeset from a \TeX/L\AA\TeX file prepared by the author.